LETTER

doi:10.1038/nature18009

Direct measurement of thermal conductivity in solid iron at planetary core conditions

Zuzana Konôpková[1]†, R. Stewart McWilliams[2], Natalia Gómez-Pérez[2,3] & Alexander F. Goncharov[4,5]

The conduction of heat through minerals and melts at extreme pressures and temperatures is of central importance to the evolution and dynamics of planets. In the cooling Earth's core, the thermal conductivity of iron alloys defines the adiabatic heat flux and therefore the thermal and compositional energy available to support the production of Earth's magnetic field via dynamo action[1–3]. Attempts to describe thermal transport in Earth's core have been problematic, with predictions of high thermal conductivity[4–7] at odds with traditional geophysical models and direct evidence for a primordial magnetic field in the rock record[8–10]. Measurements of core heat transport are needed to resolve this difference. Here we present direct measurements of the thermal conductivity of solid iron at pressure and temperature conditions relevant to the cores of Mercury-sized to Earth-sized planets, using a dynamically laser-heated diamond-anvil cell[11,12]. Our measurements place the thermal conductivity of Earth's core near the low end of previous estimates, at 18–44 watts per metre per kelvin. The result is in agreement with palaeomagnetic measurements[10] indicating that Earth's geodynamo has persisted since the beginning of Earth's history, and allows for a solid inner core as old as the dynamo.

The thermal evolution of Earth's core and the energetics of the geomagnetic field are highly sensitive[3,8,9] to the thermal conductivity of core materials at the high pressures (P) and high temperatures (T) of the core. A wide range of values for the thermal conductivity of iron (Fe) and its alloys at core conditions have been predicted using materials theory[2,4,6,7,13] and high-pressure measurements of electrical conductivity[5,14–16]. To predict thermal conductivity, the Wiedemann–Franz–Lorenz law:

$$k = LT\sigma \tag{1}$$

has almost universally been employed, where k and σ are the thermal and electrical conductivities and L is the Lorenz number. The Lorenz number—traditionally an empirically determined quantity[17]—has been calculated theoretically[6,7] but not measured for Fe or its alloys at high pressure and temperature conditions.

For low estimates of thermal conductivity[2], near $k = 30\,\mathrm{W\,m^{-1}\,K^{-1}}$, the geodynamo may be sustained during the whole life of the planet, and convection of the core is readily attained in thermal (in absence of an inner core) or thermochemical scenarios[9]. On the other hand, a recent estimate[6] near $k = 130\,\mathrm{W\,m^{-1}\,K^{-1}}$ implies a young inner core (that is, less than 1.3 billion years old), and only thermal convection driving the dynamo at earlier times[3]. However, a paradox arises[8] when evidence of an ancient magnetic field[3,10] must be reconciled with the high energy fluxes needed to drive thermal convection in a high conductivity, fully fluid core. The large core–mantle boundary heat flux (Q_{CMB}) and high internal temperatures for the early Earth in this case (implying a molten lower mantle and possibly a stably stratified core) are difficult to explain given current mantle evolution models and low present-day Q_{CMB} (ref. 3). Re-evaluating the history and energy balances of Earth's core and mantle in this context, it is necessary to have certainty on the validity of reported values of k (ref. 8). Thus, there is a pressing need for direct thermal conductivity measurements of core materials at conditions relevant to Earth's core.

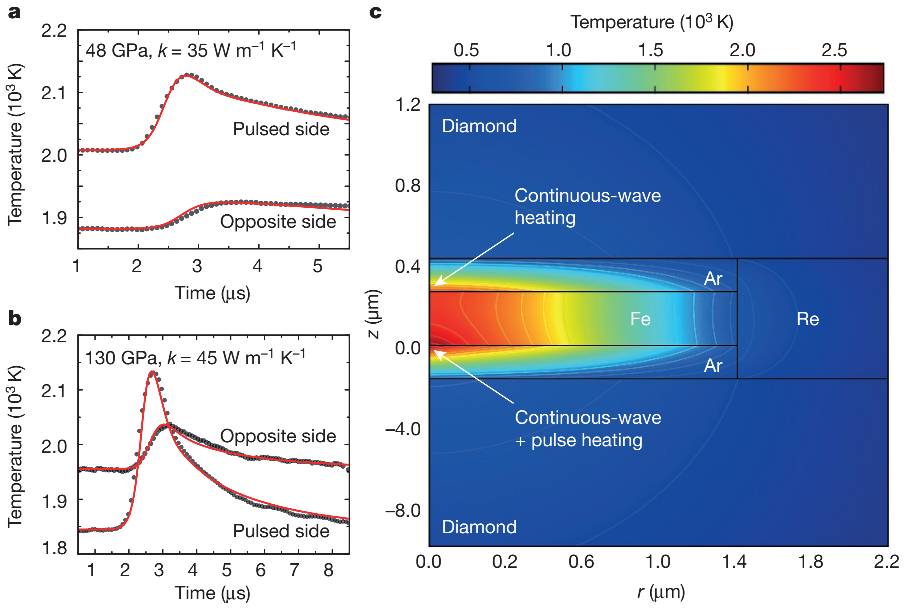

Figure 1 | Temperature of Fe foils during flash heating at high initial temperature and pressure. a, **b**, Plots of the measured temperature histories (grey) on the pulsed and opposite sides of the foil together with finite-element models (red) for best-fit thermal conductivity k of Fe, at two pressures: **a**, $P = 48$ GPa; **b**, $P = 130$ GPa. **c**, Instantaneous temperature map of the modelled sample area at initiation of flash heating at 112 GPa, as a function of radial (r) and axial (z) position. Contour lines are isotherms.

---

[1]DESY Photon Science, Notkestrasse 85, DE-22607 Hamburg, Germany. [2]School of Physics and Astronomy and Centre for Science at Extreme Conditions, University of Edinburgh, Peter Guthrie Tait Road, Edinburgh EH9 3FD, UK. [3]Departamento de Geociencias, Universidad de Los Andes, Bogotá, Colombia. [4]Key Laboratory of Materials Physics, Institute of Solid State Physics, Chinese Academy of Sciences, 350 Shushanghu Road, Hefei, Anhui 230031, China. [5]Geophysical Laboratory, Carnegie Institution of Washington, 5251 Broad Branch Road NW, Washington DC 20015, USA. †Present address: European XFEL GmbH, Notkestrasse 85, DE-22607 Hamburg, Germany.

Although the technical capability of reaching planetary core conditions in the laboratory has long been available using the laser-heated diamond-anvil cell (DAC), measurements sensitive to transport properties have been scarce. Thermal transport measurements have been especially challenging. To overcome this limitation, we dynamically measured temperature in the laser-heated DAC[11,12] to study the propagation of heat pulses across Fe foils contained at high initial pressure (35–130 GPa) and temperature (1,600–3,000 K) (Fig. 1). Fitting of the temporally and spatially resolved temperature fluctuations with heat conduction models provides a strong constraint on the thermal transport (Methods and Extended Data Figs 2–6).

The experiments performed below ~50 GPa probe Fe in the stability field of face-centred cubic γ Fe (Fig. 2)[18–22]. At conditions close to those at the centre of Mercury's core[23] (~40 GPa and 2,200–2,500 K), thermal conductivity is 35 ± 10 W m^{-1} K^{-1}. This is similar to the ambient pressure values in γ Fe ($k = 30 \pm 3$ W m^{-1} K^{-1})[24], suggesting that k is not strongly dependent on pressure at Mercury's core conditions. This result is similar to earlier expectations for the thermal conductivity of Mercury's core[25] of ~40 W m^{-1} K^{-1}, but is at odds with more recent estimates[21]. At pressures in the range 50–80 GPa, the sample is usually pre-heated in the hexagonal close-packed ε Fe phase but may undergo partial transformation to the γ phase during the thermal pulse. Thermal conductivity values found at these conditions are considered biased towards the ε phase, and are in general agreement with earlier DAC measurements on ε Fe (ref. 26). The highest-pressure data, 88–130 GPa at 1,600–3,500 K, are unambiguously in the region of ε Fe and are closest to the conditions at Earth's core–mantle boundary[1,6]: 136 GPa and 3,800–4,800 K. A large number of measurements (>20) at 112 GPa show k to decrease with temperature at these conditions (Fig. 3), as expected from combining electrical conductivity data under static and shock wave compression[14].

To model the temperature dependence of thermal conductivity in ε Fe, we fitted the data at 112 GPa to:

$$k = aT + \frac{b}{\sqrt{T}} \tag{2}$$

This form ensures a realistic behaviour of both thermal conductivity and electrical resistivity ($1/\sigma$) that is consistent with previous high-temperature resistivity data[5,14,21] (see Methods and Extended Data Fig. 1). The model fit at 112 GPa (Fig. 3) also includes resistivity data at room temperature[5,14] extrapolated to 112 GPa and shock wave resistivity data[15] interpolated to 112 GPa. These data were converted to thermal conductivity using an empirical Lorenz number of $(1.9 \pm 0.4) \times 10^{-8}$ W Ω K^{-2} (see Methods). The fit of equation (2) yields $b \approx 1{,}972$ W m^{-1} K$^{-1/2}$ and $a \approx 0$. The error in model thermal conductivities is ~20% (one standard deviation).

To assess the pressure variation of k in ε Fe, we used a physical model for the variation of electronic thermal conductivity with pressure (see Methods) in terms of isothermal bulk modulus (K_T) and Grüneisen parameter (γ):

$$\frac{1}{k}\frac{\partial k}{\partial P} = \frac{2\gamma - 1/3}{K_T} \tag{3}$$

The Grüneisen parameter and bulk modulus at core conditions are evaluated using the thermal equation of state of Fe (ref. 27) (see Methods). The model represents our data well to 130 GPa (Fig. 2), and predicts somewhat larger values of k at Earth's outer core conditions (Fig. 3). Accounting for the uncertainty in outer core temperature[1,6], k for pure Fe varies from 33 ± 7 W m^{-1} K^{-1} at core–mantle boundary conditions ($T = 3{,}800$–$4{,}800$ K, $P = 136$ GPa) to 46 ± 9 W m^{-1} K^{-1} at inner-core boundary conditions ($T = 5{,}600$–$6{,}500$ K, $P = 330$ GPa).

The conductivity of molten Fe, which is relevant to the outer core, is generally taken to be similar to that of solid Fe near melting[13,21,28]. The addition of light-element impurities is expected to reduce conductivity by 10%–40% (refs 7 and 13). Thus, the thermal conductivity for Earth's liquid outer core is between 25 ± 7 W m^{-1} K^{-1} at the core–mantle boundary and 35 ± 10 W m^{-1} K^{-1} at the inner-core boundary. Refining estimates for liquid core composition can further reduce this uncertainty. The corresponding electrical resistivity of the outer core is 3.7 ± 1.5 μΩ m.

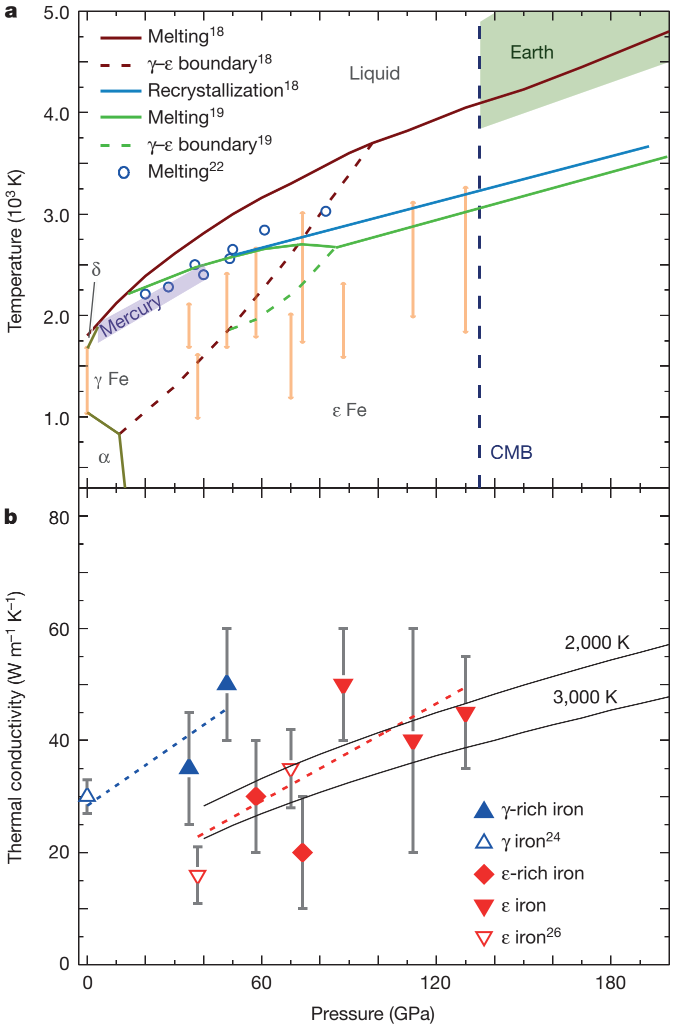

Figure 2 | Thermal conductivity of Fe at high pressure and temperature. **a**, Phase diagram[18–20,22] of Fe with conditions of the thermal conductivity measurements (orange) falling in the domain of the γ and ε phases. The shaded areas depict conditions of Earth's core[1,6] and Mercury's core[23], with the vertical dashed line marking the pressure at Earth's core–mantle boundary (CMB). **b**, Thermal conductivity results from this study are shown as solid symbols: in the domain of γ Fe (upward triangles) the γ and ε phases most probably co-exist[18]; for samples typically pre-heated to below the γ–ε boundary and then crossing it briefly during thermal pulses (diamonds), the phase is considered to be mostly ε Fe; at higher pressure (downward triangles) samples are pure ε Fe at all conditions[18] (see Methods). Prior direct thermal conductivity measurements on the γ phase[24] and the ε phase[26] are shown as open symbols. The dashed lines are linear fits to the results from the γ and ε domains, whereas solid lines are model values (see equations (2) and (3)). Error bars include uncertainty (one standard deviation) and range of measurements.

Our thermal conductivities for pure Fe at core conditions compare well with predictions based on resistivity measurements at high pressure[14] including shock wave results (52 ± 11 W m^{-1} K^{-1}) or Stacey's law of constant resistivity at melting[2] (48 ± 10 W m^{-1} K^{-1}), where the empirical value of L has been applied. Such predictions are sensitive to the assumptions used, however, and much larger values are found using slightly different approaches[5,13,14], emphasizing the need for direct constraints from high-pressure, high-temperature data. Calculations[6,7] finding $k = 120$–160 W m^{-1} K^{-1} at core–mantle boundary conditions

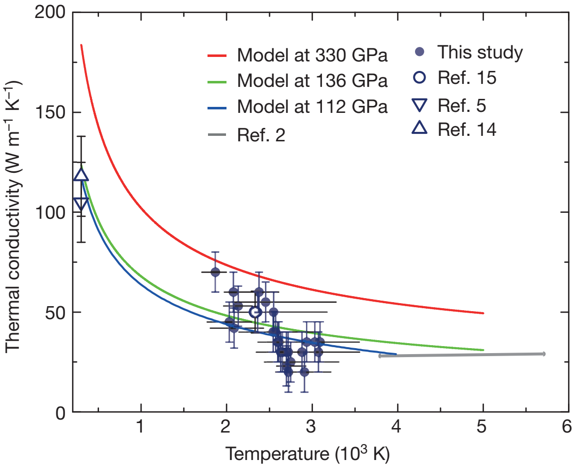

Figure 3 | Thermal conductivity of Fe versus temperature. Solid circles indicate results from this study at 112 GPa, with horizontal bars indicating the range of temperatures observed in each experiment, and vertical bars the uncertainty in k (one standard deviation). Estimates based on prior electrical resistivity measurements[5,14,15] are shown as open symbols, with bars indicating uncertainty from the empirical determination of L. The thermal conductivity model for 112 GPa, 136 GPa (core–mantle boundary), and 330 GPa (inner-core boundary) are blue, green and red lines, respectively (see equations (2) and (3)). For comparison, the prediction of ref. 2 for core alloy at outer-core conditions is the grey line.

and $k = 205$–$250\ \mathrm{W\,m^{-1}\,K^{-1}}$ at inner-core boundary conditions are 5.6 ± 1.8 and 6.5 ± 1.7 times larger than our values, respectively.

During an early stage of Earth history before the formation of the inner core, the presence of the geodynamo requires a core–mantle boundary heat flux (Q_{CMB}) greater than the conductive heat flux in the core. The heat flux requirements for such a convective early core are moderate for the values of k found in this study, similar to that of ref. 9: Q_{CMB} must exceed a threshold of 3.8 ± 1.6 TW (for k of $31 \pm 13\ \mathrm{W\,m^{-1}\,K^{-1}}$) for Earth's magnetic field to be sustained, assuming negligible radiogenic heating. Later in the planet's history, after a solid inner core has formed, the core–mantle heat flux necessary to sustain a dynamo may be smaller, given that convection can be driven both compositionally and thermally. Estimates[3] for the current Q_{CMB} (12 ± 5 TW) far exceed this threshold, so for a nominal scenario of Q_{CMB} declining or constant with time[3,9] magnetic activity is expected throughout Earth history, and would probably only have been absent when internal dynamics differed substantially from those of the present, for example in periods lacking plate tectonics[29]. Similarly, evidence of non-zero palaeomagnetic field places a hard constraint on the corresponding heat flux of $Q_{\mathrm{CMB}} > 2.2$ TW before inner-core nucleation.

However, the inner core can be older for lower core thermal conductivities[5], and within the uncertainty due to the light-element content of the core, the inner core can be as old as the earliest recorded terrestrial magnetic field[10], that is, up to 4.2 billion years old. Thus, within our direct experimental constraints, there is no requirement that Earth's geodynamo ever existed in the absence of an inner core. Indeed, the planet's dynamo and its solid inner core may have co-existed since soon after the formation of Earth. Greater knowledge of the light-element content of the core and its effect on thermal conductivity is essential to understand the earliest period of Earth's core evolution.

Online Content Methods, along with any additional Extended Data display items and Source Data, are available in the online version of the paper; references unique to these sections appear only in the online paper.

Received 30 September 2015; accepted 11 April 2016.

1. Labrosse, S. Thermal and magnetic evolution of the Earth's core. *Phys. Earth Planet. Inter.* **140,** 127–143 (2003).
2. Stacey, F. D. & Loper, D. E. A revised estimate of the conductivity of iron alloy at high pressure and implications for the core energy balance. *Phys. Earth Planet. Inter.* **161,** 13–18 (2007).
3. Nimmo, F. in *Treatise on Geophysics* 2nd edn (ed. Schubert, G.) 27–55, 201–219 (Elsevier, 2015).
4. Sha, X. & Cohen, R. First-principles studies of electrical resistivity of iron under pressure. *J. Phys. Condens. Matter* **23,** 075401 (2011).
5. Gomi, H. *et al.* The high conductivity of iron and thermal evolution of the Earth's core. *Phys. Earth Planet. Inter.* **224,** 88–103 (2013).
6. Pozzo, M., Davies, C., Gubbins, D. & Alfe, D. Thermal and electrical conductivity of iron at Earth's core conditions. *Nature* **485,** 355–358 (2012).
7. de Koker, N., Steinle-Neumann, G. & Vlcek, V. Electrical resistivity and thermal conductivity of liquid Fe alloys at high P and T, and heat flux in Earth's core. *Proc. Natl Acad. Sci. USA* **109,** 4070–4073 (2012).
8. Olson, P. The new core paradox. *Science* **342,** 431–432 (2013).
9. Nimmo, F. in *Treatise on Geophysics* (ed. Schubert, G.) 31–65, 217–241 (Elsevier, 2007).
10. Tarduno, J. A., Cottrell, R. D., Davis, W. J., Nimmo, F. & Bono, R. K. A Hadean to Paleoarchean geodynamo recorded by single zircon crystals. *Science* **349,** 521–524 (2015).
11. McWilliams, R. S., Konôpková, Z. & Goncharov, A. F. A flash heating method for measuring thermal conductivity at high pressure and temperature: application to Pt. *Phys. Earth Planet. Inter.* **247,** 17–26 (2015).
12. McWilliams, R. S., Dalton, D. A., Konôpková, Z., Mahmood, M. F. & Goncharov, A. F. Opacity and conductivity measurements in noble gases at conditions of planetary and stellar interiors. *Proc. Natl Acad. Sci. USA* **112,** 7925–7930 (2015).
13. Stacey, F. D. & Anderson, O. L. Electrical and thermal conductivities of Fe-Ni-Si alloy under core conditions. *Phys. Earth Planet. Inter.* **124,** 153–162 (2001).
14. Seagle, C. T., Cottrell, E., Fei, Y. W., Hummer, D. R. & Prakapenka, V. B. Electrical and thermal transport properties of iron and iron-silicon alloy at high pressure. *Geophys. Res. Lett.* **40,** 5377–5381 (2013).
15. Bi, Y., Tan, H. & Jing, F. Electrical conductivity of iron under shock compression up to 200 GPa. *J. Phys. Condens. Matter* **14,** 10849 (2002).
16. Keeler, R. N. & Royce, E. B. in *Physics of High Energy Density* Vol. 48 (eds Caldirola, P. & Knoepfel, H.) 106–125 (Academic Press, 1971).
17. Franz, R. & Wiedemann, G. Ueber die Wärme-Leitungsfähigkeit der Metalle. *Ann. Phys.* **165,** 497–531 (1853).
18. Anzellini, S., Dewaele, A., Mezouar, M., Loubeyre, P. & Morard, G. Melting of iron at Earth's inner core boundary based on fast X-ray diffraction. *Science* **340,** 464–466 (2013).
19. Boehler, R. Temperatures in the Earth's core from melting-point measurements of iron at high static pressures. *Nature* **363,** 534–536 (1993).
20. Komabayashi, T., Fei, Y., Meng, Y. & Prakapenka, V. In-situ X-ray diffraction measurements of the γ-ε transition boundary of iron in an internally-heated diamond anvil cell. *Earth Planet. Sci. Lett.* **282,** 252–257 (2009).
21. Deng, L., Seagle, C., Fei, Y. & Shahar, A. High pressure and temperature electrical resistivity of iron and implications for planetary cores. *Geophys. Res. Lett.* **40,** 33–37 (2013).
22. Jackson, J. M. *et al.* Melting of compressed iron by monitoring atomic dynamics. *Earth Planet. Sci. Lett.* **362,** 143–150 (2013).
23. Rivoldini, A., Van Hoolst, T. & Verhoeven, O. The interior structure of Mercury and its core sulfur content. *Icarus* **201,** 12–30 (2009).
24. Ho, C. Y., Powell, R. W. & Liley, P. E. Thermal conductivity of the elements. *J. Phys. Chem. Ref. Data* **1,** 279–422 (1972).
25. Hauck, S. A., Dombard, A. J., Phillips, R. J. & Solomon, S. C. Internal and tectonic evolution of Mercury. *Earth Planet. Sci. Lett.* **222,** 713–728 (2004).
26. Konôpková, Z., Lazor, P., Goncharov, A. F. & Struzhkin, V. V. Thermal conductivity of hcp iron at high pressure and temperature. *High Press. Res.* **31,** 228–236 (2011).
27. Dubrovinsky, L. S., Saxena, S. K., Tutti, F., Rekhi, S. & LeBehan, T. In situ X-ray study of thermal expansion and phase transition of iron at multimegabar pressure. *Phys. Rev. Lett.* **84,** 1720–1723 (2000).
28. Secco, R. A. & Schloessin, H. H. The electrical resistivity of solid and liquid Fe at pressures up to 7 GPa. *J. Geophys. Res. Solid Earth* **94,** 5887–5894 (1989).
29. Nimmo, F. & Stevenson, D. J. Influence of early plate tectonics on the thermal evolution and magnetic field of Mars. *J. Geophys. Res. Planets* **105,** 11969–11979 (2000).

Acknowledgements We acknowledge experimental assistance from H. Marquardt. This work was supported by the NSF (grant numbers DMR-1039807, EAR-1015239, EAR-1520648 and EAR/IF-1128867), the Army Research Office (grant 56122-CH-H), the Carnegie Institution of Washington, the National Natural Science Foundation of China (grant number 21473211), the Chinese Academy of Science (grant number YZ201524), the University of Edinburgh, and the British Council Researcher Links Programme. Portions of this research were carried out at the light source Petra III at DESY, a member of the Helmholtz Association (HGF).

Author Contributions Z.K., R.S.M. and A.F.G. designed and conducted experiments. R.S.M. reduced raw data. Z.K. and N.G.P. performed finite-element modelling. N.G.P. performed error analysis and geophysical calculations. All authors wrote the manuscript.

Author Information Reprints and permissions information is available at www.nature.com/reprints. The authors declare no competing financial interests. Readers are welcome to comment on the online version of the paper. Correspondence and requests for materials should be addressed to Z.K. (zuzana.konopkova@xfel.eu), R.S.M. (r.s.mcwilliams@ed.ac.uk), N.G.-P. (ngomez@uniandes.edu.co) or A.F.G. (alex@issp.ac.cn).

METHODS

Briefly, a high-purity Fe foil (99.99%, GoodFellow) placed between two anvils of the DAC and separated from the anvils by layers of insulating material (NaCl or Ar) was preheated to a desired stable temperature using double-sided continuous-wave infrared laser heating, and then pulse-heated on one side with an additional infrared laser to create a thermal disturbance[11]. The evolution of this disturbance was characterized by nanosecond-resolved radiative temperature measurements using a streak camera coupled to a grating spectrograph that records the thermal incandescent history from both sides of the foil. The phase shift and the reduction in amplitude of the temperature disturbance as it propagates across the foil are thus measured[11]. At a given pressure, a series of data sets were collected using different continuous-wave and pulse laser powers. Temperatures studied ranged from ~1,600 K, the lowest detectable temperature, to 4,000 K at the maximum, whereas temperature disturbances were typically a few hundred kelvin in amplitude.

The temperature evolution was fitted to time-dependent finite-element models of the laser-heated DAC[11,26,30] to determine the thermal conductivity of Fe samples. For the finite-element modelling we employed experimentally determined geometrical parameters and thermochemical parameters determined from known equations of state. The thermal conductivity of the sample, together with the thermal conductivity of the pressure medium and heating power, were adjusted until the best match of modelled and experimental temperature was achieved (Fig. 1a). The analysis was rigorously tested for sensitivity to input parameters (Extended Data Figs 2, 3 and 6). Total uncertainty and error bars (Fig. 2) were determined from the fitting uncertainty (Extended Data Figs 2 and 5), the scatter across different data sets (for example, Fig. 3), and uncertainty in input parameters (Extended Data Figs 3 and 6). We find the measurements to be sufficiently sensitive to the thermal conductivity of the sample foil to provide a major constraint on Fe conductivity at core conditions.

The experiment duration (less than 10 s per temperature history collection) was kept as short as possible to avoid sample damage and minimize the heating of optics and DAC that could cause instabilities during long laser-heating runs. Foil initial thickness ($4.01 \pm 0.02\,\mu$m) and *in situ* thickness (Extended Data Table 1) were measured using white-light interferometry of the DAC cavity, and the index of refraction data for the media under pressure[31–33]; these measurements also determined the sample-to-diamond-culet distances, which are important parameters in finite-element calculations. Foil thickness changes measured under compression were consistent with those derived from the known compressibility of Fe[34]. For the NaCl medium, insulation plates were formed and placed on the culets, and foils were placed between them; in the case of Ar, the foil was suspended on a recess in the gasket (Re).

A sample of platinum, which has well defined thermal conductivity behaviour[11] at high pressure and temperature, was available as a control in some experiments at low pressures where the DAC cavities were sufficiently large in diameter ($P \leq 55$ GPa) to accommodate a second foil. The Pt foil had the same thickness as the Fe foil, and was positioned on the plane of the Fe foil in the cavity; for such foil pairs, sample and insulation thicknesses, cell geometry, pressure, medium, heating configuration, and detection system were identical, allowing a direct relative comparison between the thermal transport behaviour of the two materials. Heat wave propagation across the Pt was much faster than for Fe (for example, 240 ns for the half-rise time, compared to 565 ns in Fe at 48 GPa; see Extended Data Fig. 4), corresponding to a lower thermal diffusivity for Fe. Fe samples were also observed to sustain larger axial temperature gradients than the Pt samples, manifested in a greater difference between peak amplitudes on either side of the foil. These observations affirm that at the studied conditions, the thermal conductivity of Pt ($160 \pm 40\,\mathrm{W\,m^{-1}\,K^{-1}}$; ref. 11) is substantially greater than that of Fe.

The Lorenz number for ε Fe was determined by comparing shock wave electrical resistivity[15] and the present thermal conductivity data at comparable pressure and temperature (Fig. 3). The result is 22 ± 16% lower than the value for a free-electron metal[35] ($L = 2.44 \times 10^{-8}\,\mathrm{W\,\Omega\,K^{-2}}$), consistent with theoretical calculations[7], which predict a Lorenz number reduced from the ideal by up to 17%.

Experimental details. To generate thermal perturbations at high initial pressure and temperature, we combined double-sided continuous and single-sided pulsed laser heating of the DAC sample[11]. The initial temperature was reached by balancing laser power to either side of the sample until temperatures agreed to within ~100 K, and then pulsed heating was used to create a small perturbation in temperature which propagated across the sample. Our approach is similar to that used in traditional flash heating measurements of thermal diffusivity[36], modified for a specimen under pressure in a DAC[11]. The reduction in amplitude and phase shifting of the heat pulse with distance is an essentially one-dimensional phenomenon[11,36], whereas two-dimensional effects have a secondary, but non-negligible, impact accounted for via finite-element modelling.

Precise temperature determination during pulse laser heating was made with a streak camera detecting system coupled to a spectrometer, capable of detecting thermal emission in a time-resolved manner in a spectrogram. Spectrograms (3–10 μs) were synchronized to the heating pulses to follow the sample's temperature response on both sides. Thermal emission was fitted to a greybody Planck function assuming constant emissivity during the heat cycle[11], a reasonable approximation since thermal perturbations are small. The time resolution of the temperature measurements was 26 ns (3-μs sweep) to 82 ns (10-μs sweep). Spectrograms were integrated over 10^2 to 10^4 perturbation cycles, at a rate of 1 kHz and total integration times of 0.1–10 s, the total integration time depending on temperature. Emission was calibrated to a tungsten ribbon lamp of known radiance. Temperatures were detected only above ~1,600 K owing to a lack of signal at lower temperatures. Experiments were limited at high temperatures owing to visible foil deformation in the melting regime of the sample and pressure medium[11].

Pressure was measured by the ruby fluorescence technique at room temperature. Thermal pressures produced during laser heating are positive but small (of the order of a few gigapascals) in sample configurations similar to those used here[18] and do not significantly affect our results.

At pressures and temperatures in the stability field of γ Fe, face-centred cubic γ Fe and hexagonal close-packed ε Fe are commonly observed to coexist in experiments[18]. Consequently, our data at these conditions may probe a mixed state of γ Fe and ε Fe with a variable γ Fe composition (Fig. 2). In contrast, at higher pressures, ε Fe is typically the only observed solid phase at all temperatures[18,37], so our data in this regime directly probe pure ε Fe. To test these expectations, we have also performed *in situ* X-ray diffraction measurements on laser-heated Fe samples prepared in a manner identical to that used in this study (with NaCl media), at the P02.2 beamline (ECB) of PETRA III in Hamburg. Using comparable timescales of heating, we confirm that a mixed phase should be present in the lower-pressure experiments reported in this study, but not at higher pressures.

To prevent the uptake of impurities in our initially high-purity Fe foils, pressure-medium materials (NaCl, Ar) were chosen and carefully prepared so that reactions with the sample are avoided[38,39]. During preparation, Fe foils and NaCl media and were kept dry, and contact with the atmosphere was minimized to prevent foil oxidation. Carbon from diamond anvils is known to react with Fe at high pressures and temperatures in laser-heated DAC experiments, but generally at much higher temperatures (and longer timescales) than probed in this work[18,37]. In testing our sample preparation and heating technique in separate *in situ* X-ray diffraction experiments, we ruled out oxidation or reaction with the medium, and confirmed that carbide formation occurs at much higher temperatures and longer heating timescales than we have used here. Thus, our Fe samples should remain very pure at the pressures, temperatures, and timescales of this study. Analysis of the recovered sample from experiments at 58–74 GPa (using electron imaging, energy dispersive scattering for chemical analysis, and a focused ion beam to section the foil at heated regions) found no detectable local enrichment of impurities in the heated areas of the sample, indicating bulk impurity levels well below detection limits (≤0.6 wt% C, ≤0.6 wt% O, ≤100 parts per million Ar), consistent with expectations from X-ray diffraction. Finally, no systematic changes in measured conductivities were observed with heating time, indicating that samples did not undergo any progressive transformation (such as a reaction) that influenced the thermal conductivity.

Model for pressure variation of thermal conductivity. The model used here to estimate pressure variation of thermal conductivity (equation (3)) is based on a formal differentiation of the electronic thermal resistivity ($W_e = 1/k_e$) with respect to density combined with the definition of the Grüneisen parameter ($\gamma = (\partial \ln\theta_D / \partial \ln\rho)_T$, where θ_D is the Debye temperature, and ρ is density), which leads to[40]:

$$\left(\frac{\partial \ln W_e}{\partial \ln\rho}\right)_T = -2\gamma + \left(\frac{\partial \ln C}{\partial \ln\rho}\right)_T \qquad (4)$$

where C is a constant containing lattice and band structure information originating from the Bloch–Grüneisen expression. Bohlin[41] finds $(\partial \ln C / \partial \ln\rho)_T$ to be equal to $-1/3$ in ordinary pure metals; the variation of electronic thermal conductivity with pressure can then be expressed in terms of the isothermal bulk modulus (K_T) and the Grüneisen parameter (γ) as equation (3).

The Grüneisen parameter of Fe is fairly well known at high pressure and room temperature: the data of refs 42 and 43 agree well, particularly above 100 GPa. At core conditions (high T), $\gamma(P, T)$ and $K_T(P, T)$ were evaluated using a thermal equation of state of Fe (ref. 27), with $\gamma = \gamma_0 \left(\frac{V}{V_0}\right)^q$, where $\gamma_0 = 1.78$, $q = 0.69$ and $V_0 = 6.73\,\mathrm{cm^3\,mol^{-1}}$. The P, T description of γ is expressed in a polynomial form:

$$\gamma(P, T) = \frac{a + cP + eT + gP^2 + iT^2 + kPT}{1 + bP + dT + fP^2 + hT^2 + jPT} \qquad (5)$$

We described $K_T(P, T)$ by the following equation:

$$K_T(P,T) = K_1 + \frac{K_2 P}{\ln(P)} + \frac{K_3 T}{\ln(T)} \tag{6}$$

All the coefficients for γ and K_T (equations (5) and (6)) are given in Extended Data Table 2.

This model gives good agreement with ε Fe electrical resistivity data at lower pressures and ambient temperatures[5,14], fits the present thermal conductivity results for ε Fe well (Fig. 2), and implies that thermal conductivity is only weakly pressure dependent above 100 GPa, consistent with prior expectations[2]. Thus, our measurements, taken at pressures close to those at the top of Earth's core, should constrain overall core conductivity accurately.

The Lorenz number for ε Fe. The temperatures and pressures of our thermal conductivity measurements overlap with those of shock wave electrical resistivity measurements[15], allowing a comparison between the resistivity and thermal conductivity measurements to obtain an empirical value for L.

At 112 GPa, where the most extensive high temperature data set was available in the present results, electrical conductivity was estimated as follows using the data of ref. 15. The two lowest pressure points from that study at 101.1 GPa and 146.7 GPa are solid-state data and so are comparable to the present results; a higher pressure point corresponds to the liquid[15,18]. First, a temperature for the middle of the three data points (146.7 GPa, 3,357 K) after isentropic release from the initial conditions (173.4 GPa, 3,552 K)—not reported—was estimated from the scaling of release behaviour reported by ref. 15; release temperatures were confirmed by independent calculation using an ε Fe equation of state[34]. The electrical conductivity at 112 GPa is then estimated as $(1.13 \pm 0.11) \times 10^6\,\mathrm{S\,m^{-1}}$ at 2,332 K, based on a linear interpolation between the solid-state data points, and assuming an uncertainty of ~10%, consistent with uncertainties reported for similar measurements[16] and scatter in the data reported by ref. 15. At this temperature in our experiments, $k = 50 \pm 10\,\mathrm{W\,m^{-1}\,K^{-1}}$ (Fig. 3). The corresponding value of L is then $(1.9 \pm 0.4) \times 10^{-8}\,\mathrm{W\,\Omega\,K^{-2}}$, 22 ± 16% less than the standard value for a free-electron metal. This correction has a small influence on our analysis. For example, assuming the free-electron value of L, the shock wave results of ref. 15 imply a value of $67\,\mathrm{W\,m^{-1}\,K^{-1}}$ at 112 GPa and 2,330 K, only slightly above the measured value.

The correction to the standard value of L determined here for ε Fe is typical for Fe at various conditions and phases[7,14,24,44] (±30%) and is similar to other transition metals[11,45]. In Pt, L is measured[11] to deviate from the ideal value by ±30% at temperatures up to 2,000 K. For Mo, deviations of −10% to −30% are predicted at high temperature[45]. The variation of L across transition metals at low temperature alone is large[46], with values such as in Cu (−9%) and W (+31%).

We note that early shock data on Fe electrical resistivity at high pressures[16] finding systematically higher electrical conductivities compared to later work[15], cannot be considered to agree with our measurements, as an unrealistically large reduction in the Lorenz number would be needed. It has been proposed that spurious values were obtained in the earlier studies[16] at higher pressure ($P > 50$ GPa) owing to insulator–conductor transformation of epoxies used in target construction, an effect avoided in later measurements[15].

Model for temperature variation of thermal conductivity. Equation (2) was selected in consideration of the observed variation of electrical conductivity in ε Fe with temperature[5,14]. Electrical conductivity is modelled as following a relationship:

$$\sigma = \sigma_0 + AT^n \tag{7}$$

where $n = -1$ is typically assumed for metals at high temperatures as in the Bloch–Grüneisen model[5,7,13,14]. A value closer to $n = -1.3$ has been suggested for Fe at high pressures from resistivity measurements, under both shock and static loading, which probed temperatures and pressures similar to those examined here[14]. Similarly, fitting equation (7) to resistivity data under external heating of statically compressed samples[5], for which temperatures are particularly accurate, yielded values of $n = -1.50 \pm 0.07$, $\sigma_0 = (1.04 \pm 0.46) \times 10^6$, $A = (6.51 \pm 2.2) \times 10^{10}$, for σ in units of siemens per metre and T in units of kelvin (Extended Data Fig. 1a).

Then, considering the Wiedemann–Franz relation (equation (1)), we can write:

$$k = L(T\sigma_0 + AT^{1+n}) \tag{8}$$

leading to the empirical form in equation (2). We chose here $n = -1.5$, though results are not significantly different selecting $n = -1.3$.

Equation (2) is fitted to the present measurements at 112 GPa together with shock wave resistivity data[15], interpolated to 112 GPa as discussed above, and static resistivity data[5,14] extrapolated to 112 GPa using a double-exponential fit of the form:

$$\frac{1}{\sigma} = \alpha + \beta_1 \exp(\tau_1 P) + \beta_2 \exp(\tau_2 P) \tag{9}$$

An initial fit gave $a = (0.89 \pm 1.33) \times 10^{-3}\,\mathrm{W\,m^{-1}\,K^{-2}}$, $b = 2{,}040 \pm 140\,\mathrm{W\,m^{-1}\,K^{-1/2}}$. The linear component of the fit is nearly zero, thus a reasonable simplified version of this model for Fe is:

$$k = b' / \sqrt{T} \tag{10}$$

where $b' = 1{,}972 \pm 83\,\mathrm{W\,m^{-1}\,K^{-1/2}}$ (Fig. 3 and Extended Data Fig. 1b).

The model captures a decrease in the thermal conductivity with temperature, which is seen in the present measurements and also implied by the prior resistivity data[5,14,15] (Fig. 3). In terms of electrical resistivity (Extended Data Fig. 1c), the scaling with temperature obtained by the model compares well with that observed by ref. 5 in ε Fe at lower pressures, and shows a similar dependence to that seen in γ Fe (or possibly in the γ–ε mixed phase) at high temperatures[21]. It is seen that ε Fe up to 112 GPa has higher resistivity than γ Fe (or its mixed phase) at lower pressure (Extended Data Fig. 1c), consistent with our experimental observation of higher thermal conductivity in γ Fe compared to ε Fe in the low-pressure region (Fig. 2).

We note that the minimum measured thermal conductivity is in close agreement with values expected at traditional resistivity saturation[5] (Extended Data Fig. 1b); however, as resistivity saturation in Fe at extremes has not been clearly confirmed by theoretical studies and since available saturation models[5] cannot satisfactorily describe the data, we conclude that at present there is no reason to adopt that resistivity saturation has occurred. Assuming it has, then ε Fe at temperatures above ~3,000 K is saturation-dominated, such that thermal conductivities at core conditions would be somewhat higher (60–$80\,\mathrm{W\,m^{-1}\,K^{-1}}$) than assessed by the present modelling; however, this upper bound on conductivity is still low compared to many prior estimates, and would not substantially alter our main conclusions.

Error assessment in the thermal conductivity determination. The laser-heated DAC in combination with numerical simulations has been shown to be a promising tool for studying heat transfer at high pressures and temperatures[11,12,26,30,47–50]. This approach requires a detailed understanding of heat transfer in the DAC, including quantitative relationships between the temperature distribution, pressure chamber geometries and sample physical properties.

Finite-element model fits to temperature histories were generally performed using a manual adjustment of model parameters. This approach was evaluated against a Levenberg–Marquardt least-squares minimization of the finite-element model variables (Extended Data Fig. 5). This automatic optimization was able to improve fit quality but the improvement was not statistically significant. Furthermore, as a good initial guess was required, this additional step only added to the processing time, and was therefore not used for all data sets.

In the present study, all input parameters in modelling were carefully examined for their effect on the determination of sample thermal conductivity (Extended Data Figs 2 and 3). Uncertainties in the input parameters (such as pressure chamber geometry) were in this way included in our overall uncertainty determination for k. The heat capacity C_P of the pressure medium has a negligible effect (Extended Data Fig. 3a). For C_P of Fe we derived a range of values of 500–$700\,\mathrm{J\,kg^{-1}\,K^{-1}}$ from equations of state for ε Fe (refs 34 and 51) and other estimates[52]. Within this range, the resulting sample k is unaffected (Extended Data Fig. 3b). Thermal conductivity of the diamond anvils, temperature dependence of thermal conductivity of the pressure medium, and smaller or larger laser beam size (by about 13%) also have negligible effects on the sample k (Extended Data Fig. 3c–e). Sample and insulation layer thicknesses, on the other hand, contribute to the uncertainty in sample k: an approximately ±20% change in thicknesses leads to $\pm 7\,\mathrm{W\,m^{-1}\,K^{-1}}$ changes in sample k (Extended Data Fig. 3f–i). We assume a constant value of k for the foil in our simulations, but no significant change in results is obtained using a temperature-dependent k (Extended Data Fig. 3j).

To check potential couplings between the uncertainties in the input parameters, we have also propagated uncertainty in our input parameters in a more rigorous manner using a Monte Carlo approach (Extended Data Fig. 6). To do this, we considered only parameters which were identified as having a first-order impact on the measurements: the thicknesses of the medium on both sides of the sample, and the sample thickness. We performed 64 Monte Carlo samples within the Gaussian probability distributions of the thickness parameters, given standard deviations of 30% in each, for a representative experiment at 130 GPa (see Extended Data Fig. 6a). For each sampling, the data was fitted automatically (Extended Data Fig. 5) to determine the two thermal conductivities and the powers for the three lasers (Extended Data Fig. 6b). The distribution in the values for k of Fe has a standard deviation comparable to our single-point error (Extended Data Fig. 6d).

While suitably sensitive to the thermal conductivity of the foil, our measurements are less sensitive to the thermal conductivity of the insulating medium, which is included as a variable in fitting (usually as a constant) but which had values more sensitive to the assumed sample geometry (thickness of the insulation layers), laser beam diameter and laser power. Thus, the conductivities of insulating media are not reported, as they are not robustly determined by our approach. For Ar, the values of k obtained in the fits were generally in the range of 50–100 W m^{-1} K^{-1}, consistent with previously reported values[49].

30. Montoya, J. A. & Goncharov, A. F. Finite element calculations of the time dependent thermal fluxes in the laser-heated diamond anvil cell. *J. Appl. Phys.* **111,** 112617 (2012).
31. Johannsen, P. G. Refractive index of the alkali halides. 1. Constant joint density of states model. *Phys. Rev. B* **55,** 6856–6864 (1997).
32. Grimsditch, M., Letoullec, R., Polian, A. & Gauthier, M. Refractive index determination in diamond anvil cells: results for argon. *J. Appl. Phys.* **60,** 3479–3481 (1986).
33. Chen, B. *et al.* Elasticity, strength, and refractive index of argon at high pressures. *Phys. Rev. B* **81,** 144110 (2010).
34. Dewaele, A. *et al.* Quasihydrostatic equation of state of iron above 2 Mbar. *Phys. Rev. Lett.* **97,** 215504 (2006).
35. Sommerfeld, A. Zur Elektronentheorie der Metalle auf Grund der Fermischen Statistik. *Z. Phys.* **47,** 1–32 (1928).
36. Parker, W. J., Jenkins, R. J., Abbott, G. L. & Butler, C. P. Flash method of determining thermal diffusivity, heat capacity, and thermal conductivity. *J. Appl. Phys.* **32,** 1679 (1961).
37. Tateno, S., Hirose, K., Ohishi, Y. & Tatsumi, Y. The structure of iron in Earth's inner core. *Science* **330,** 359–361 (2010).
38. Shen, G., Prakapenka, V. B., Rivers, M. L. & Sutton, S. R. Structure of liquid iron at pressures up to 58 GPa. *Phys. Rev. Lett.* **92,** 185701 (2004).
39. Goncharov, A. F. *et al.* X-ray diffraction in the pulsed laser heated diamond anvil cell. *Rev. Sci. Instrum.* **81,** 113902 (2010).
40. Ross, R. G., Andersson, P., Sundqvist, B. & Backstrom, G. Thermal conductivity of solids and liquids under pressure. *Rep. Prog. Phys.* **47,** 1347 (1984).
41. Bohlin, L. Thermal conduction of metals at high pressure. *Solid State Commun.* **19,** 389–390 (1976).
42. Sharma, S. K. Debye temperature of hcp iron at extreme compression. *Solid State Commun.* **149,** 2207–2209 (2009).
43. Dubrovinsky, L. S., Saxena, S. K., Dubrovinskaia, N. A., Rekhi, S. & Le Bihan, T. Gruneisen parameter of ε-iron up to 300 GPa from in-situ X-ray study. *Am. Mineral.* **85,** 386–389 (2000).
44. Van Zytveld, J. Electrical resistivities of liquid transition metals. *J. Phys. Coll.* **41,** C8-503-C8-506 (1980).
45. French, M. & Mattsson, T. R. Thermoelectric transport properties of molybdenum from ab-initio simulations. *Phys. Rev. B* **90,** 165113 (2014).
46. Kittel, C. *Introduction to Solid State Physics* 8th edn (John Wiley & Sons, 2005).
47. Panero, W. R. & Jeanloz, R. Temperature gradients in the laser-heated diamond anvil cell. *J. Geophys. Res. Solid Earth* **106,** 6493–6498 (2001).
48. Kiefer, B. & Duffy, T. S. Finite element simulations of the laser-heated diamond-anvil cell. *J. Appl. Phys.* **97,** 114902 (2005).
49. Goncharov, A. F. *et al.* Thermal conductivity of argon at high pressures and high temperatures. *J. Appl. Phys.* **111,** 112609 (2012).
50. Beck, P. *et al.* Measurement of thermal diffusivity at high pressure using a transient heating technique. *Appl. Phys. Lett.* **91,** 181914 (2007).
51. Yamazaki, D. *et al.* P-V-T equation of state for ε-iron up to 80 GPa and 1900 K using the Kawai-type high pressure apparatus equipped with sintered diamond anvils. *Geophys. Res. Lett.* **39,** L20308 (2012).
52. Hirose, K., Labrosse, S. & Hernlund, J. Composition and state of the core. *Annu. Rev. Earth Planet. Sci.* **41,** 657–691 (2013).

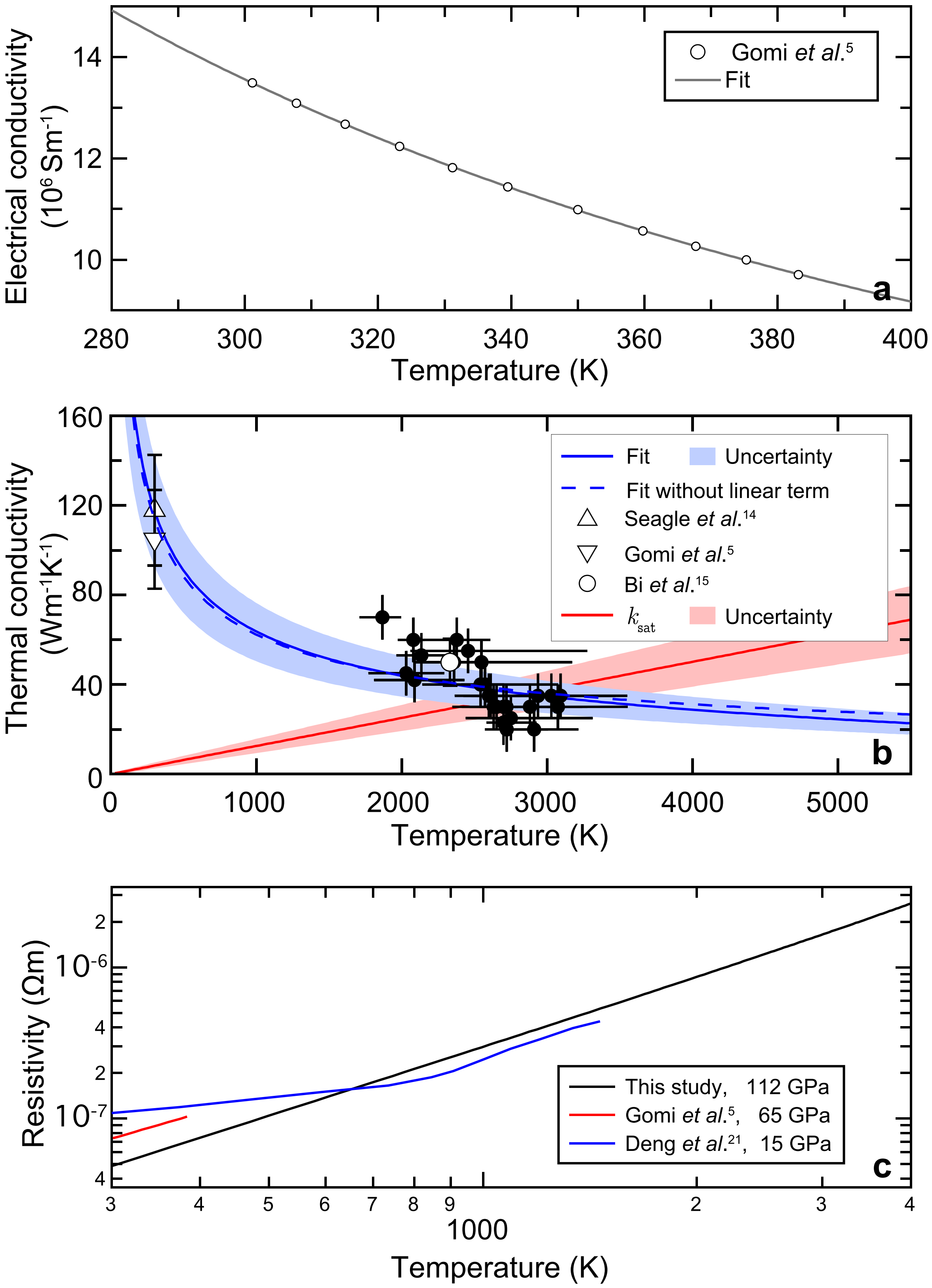

Extended Data Figure 1 | High-temperature transport properties of Fe. a, Graph of the electrical conductivity[5] as a function of temperature of ε Fe at 65 GPa and model fit (to equation (7)). **b**, Thermal conductivity temperature dependence at 112 GPa. The model fit (to equation (2), solid line) and a 20% uncertainty envelope are in blue; the model fit without linear term (to equation (10)) is a dashed blue line. Present data are solid circles and data derived from prior electrical resistivity measurements[5,14,15] are open symbols (see Fig. 3). The red band is the minimum thermal conductivity assuming resistivity saturation[5]. **c**, Electrical resistivity at several pressures, for multiple phases at 15 GPa (blue)[21], and the ε phase at 65 GPa (red)[5] and 112 GPa (this study, black).

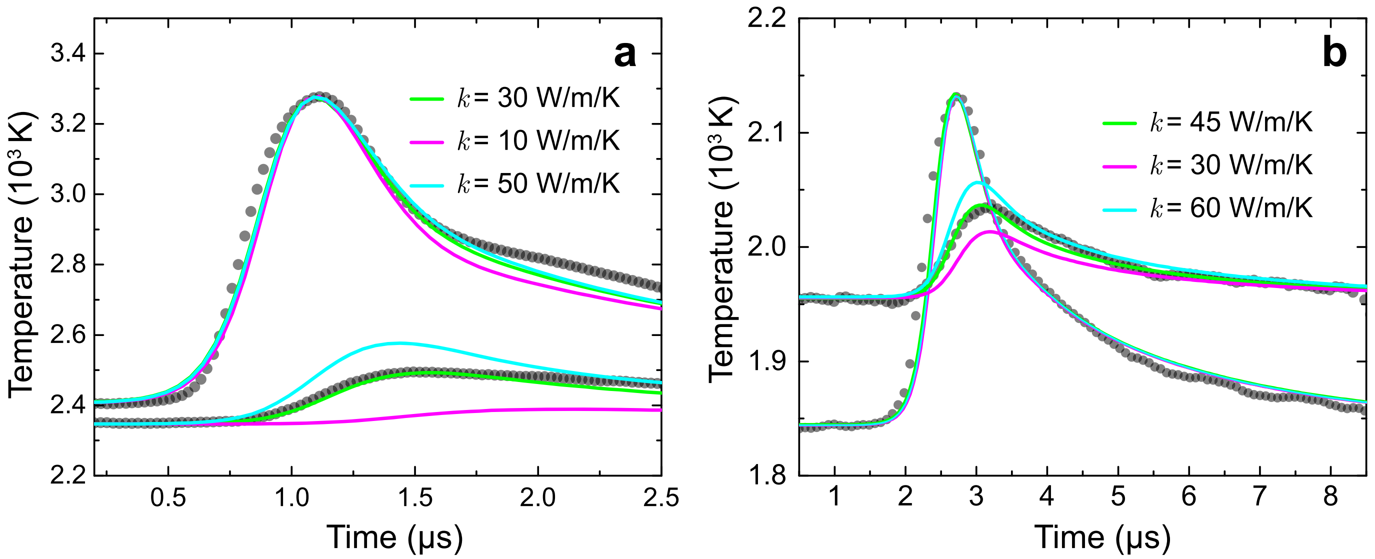

Extended Data Figure 2 | Comparison between measurements and models for different values of thermal conductivity. Data for pulsed and opposite sides of the foil are dots; the larger temperature excursion is on the pulsed side. Green, magenta and cyan curves are simulations with different values of sample k, all other parameters being held constant. The data sets at 112 GPa (**a**) and 130 GPa (**b**) have been measured using 3-μs and 10-μs sweep windows, respectively.

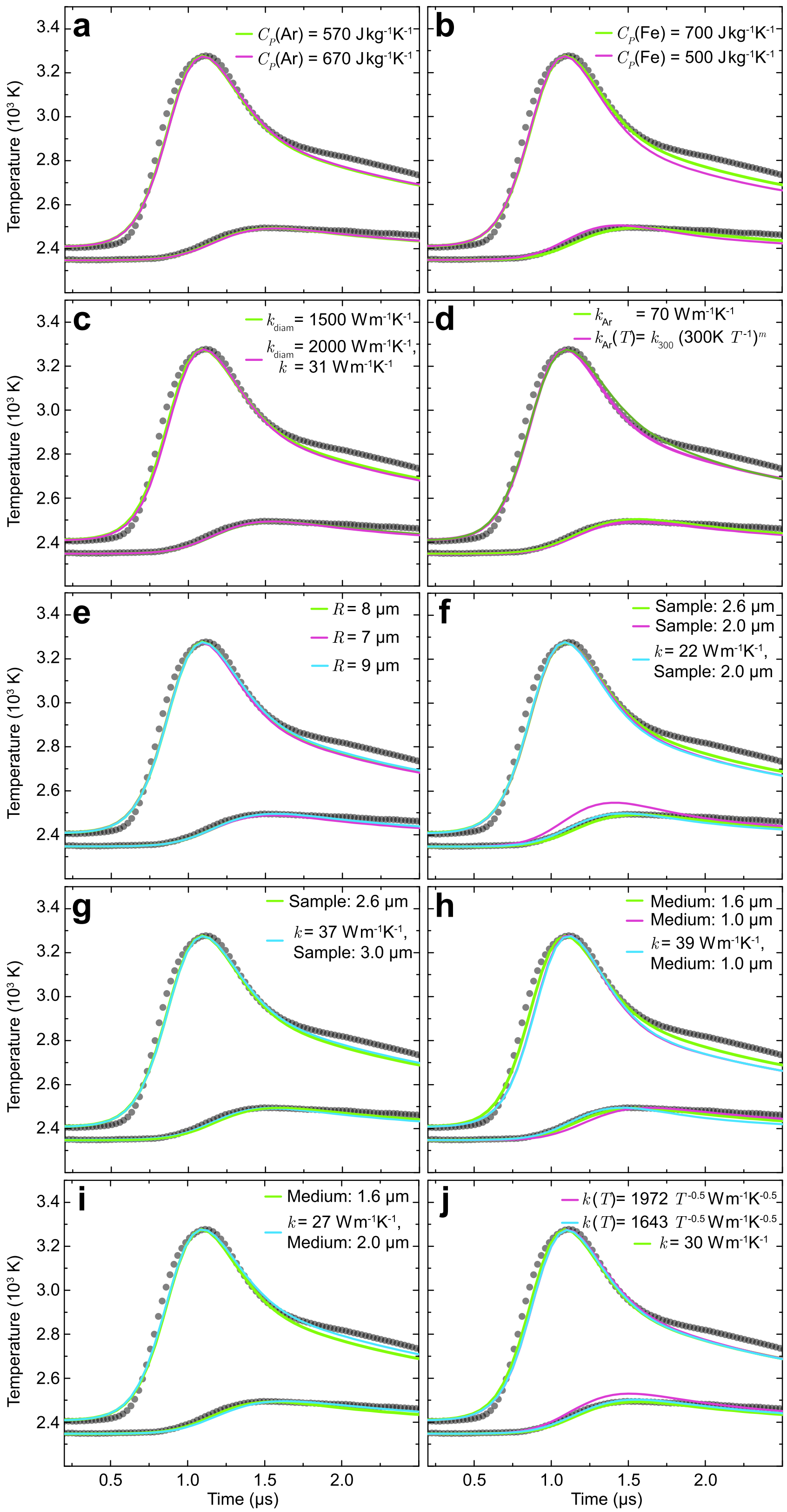

Extended Data Figure 3 | See next page for caption.

Extended Data Figure 3 | Tests of the sensitivity of finite-element model results to input parameters for an example run at 112 GPa. This experiment shows a large amplitude of temperature modulation that accentuates the effects of parameter changes. A best-fit value of $k = 30\,\mathrm{W\,m^{-1}\,K^{-1}}$, obtained using parameters listed in Extended Data Table 1, is obtained from these model fits unless stated otherwise. **a**, Effect of heat capacity of the Ar pressure medium. Uncertainty in medium C_P has no effect on k of the sample. **b**, Effect of heat capacity of the sample. Temperature profiles for two values of C_P of Fe ($500\,\mathrm{J\,kg^{-1}\,K^{-1}}$ and $700\,\mathrm{J\,kg^{-1}\,K^{-1}}$) indicate that results are only weakly affected by the uncertainty in C_P for Fe. **c**, Change in the thermal conductivity value of diamond anvils from $1{,}500\,\mathrm{W\,m^{-1}\,K^{-1}}$ to $2{,}000\,\mathrm{W\,m^{-1}\,K^{-1}}$ requires an increase in thermal conductivity of the sample from $30\,\mathrm{W\,m^{-1}\,K^{-1}}$ to $31\,\mathrm{W\,m^{-1}\,K^{-1}}$. **d**, Effect of using a T-dependent k of the medium. After ref. 49, a dependence $k(T) = k_{300}(300/T)^m$ is used, where k_{300} is the 300-K conductivity, T is in kelvin, and m is an exponent (of order 1); k_{300} ($300\,\mathrm{W\,m^{-1}\,K^{-1}}$) is extrapolated from prior results at lower pressure[49] and m (0.7) is fitted to the present data. No change in sample k is indicated using this or any other $k(T)$ model we tested for the media. **e**, Laser beam radius change of ±13% does not affect the temperature noticeably. **f**, A sample thinner by 23% (reduced from $2.6\,\mu\mathrm{m}$ to $2.0\,\mu\mathrm{m}$) would require a lower sample k of $22\,\mathrm{W\,m^{-1}\,K^{-1}}$. **g**, A sample thicker by 15% (increased from $2.6\,\mu\mathrm{m}$ to $3.0\,\mu\mathrm{m}$) would require an increased sample k of $37\,\mathrm{W\,m^{-1}\,K^{-1}}$. **h**, The insulation layer was decreased on both sides by 38%, from $1.6\,\mu\mathrm{m}$ to $1.0\,\mu\mathrm{m}$. Sample k had to increase to $39\,\mathrm{W\,m^{-1}\,K^{-1}}$. **i**, The insulation layer was increased on both sides by 25%, from $1.6\,\mu\mathrm{m}$ to $2.0\,\mu\mathrm{m}$. Sample k had to decrease to $27\,\mathrm{W\,m^{-1}\,K^{-1}}$. **j**, Effect of including T dependence of sample k in models. The temperature profile calculated using our global fit at 112 GPa (equation (2)) is shown as a magenta line; this dependence scaled within its uncertainty (reduced by a factor of 0.83) to improve the fit is shown as a cyan line. The resulting sample k varies between $24\,\mathrm{W\,m^{-1}\,K^{-1}}$ and $35\,\mathrm{W\,m^{-1}\,K^{-1}}$ in the T range of the experiment; the estimate assuming constant sample k is the average of these values.

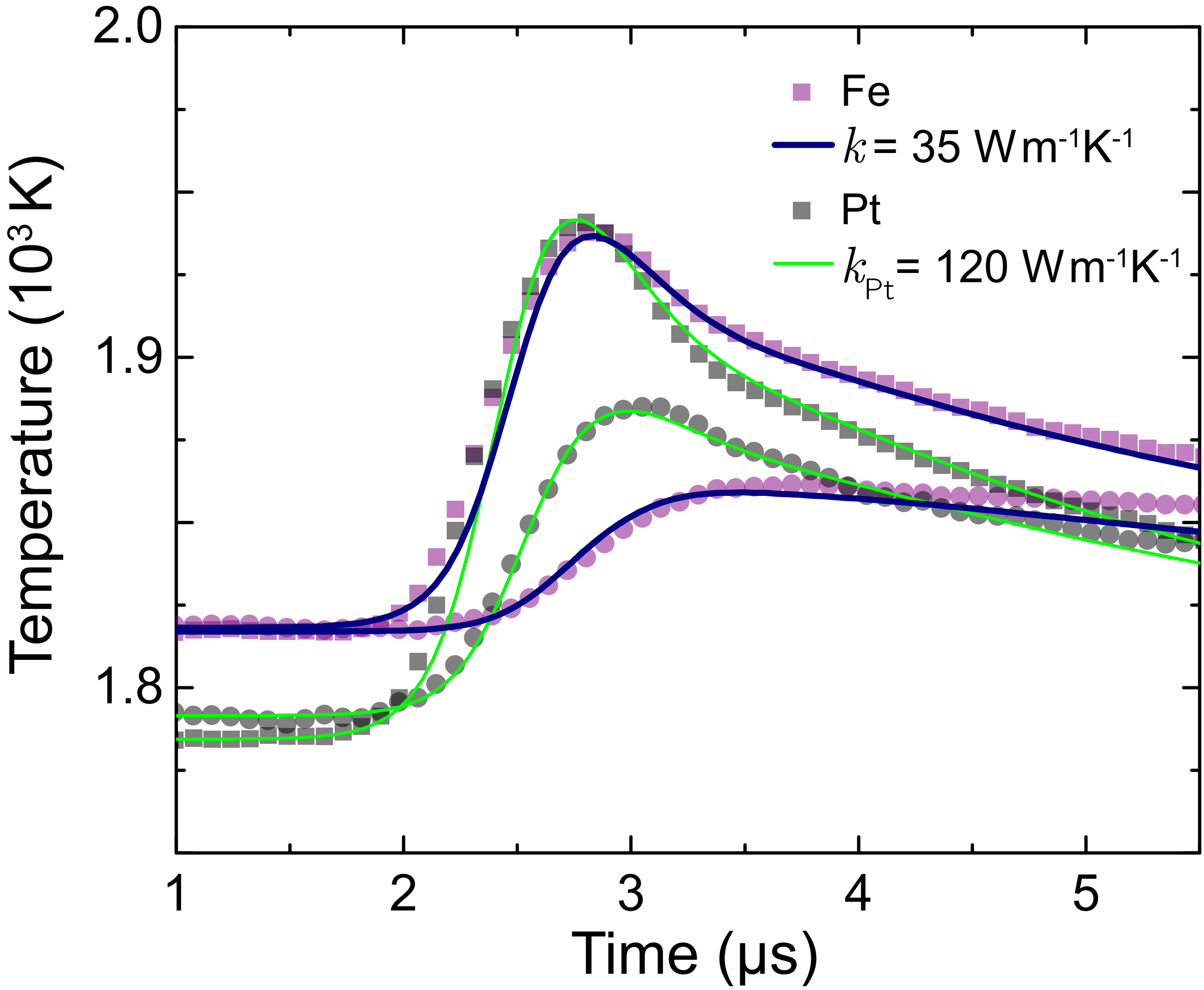

Extended Data Figure 4 | Comparison of data on Fe and Pt at 48 GPa for an identical sample configuration. The data clearly show slower propagation of heat across the Fe foil compared to Pt (ref. 11), as given by the half-rise time τ. This observation directly shows that thermal diffusivity $\kappa = (k/\rho C_P)$ of Fe is much less than Pt, since[11,36] $\kappa \propto 1/\tau$. Similarly, the smaller amplitude of the perturbation upon opposite surface arrival indicates a smaller k in Fe than in Pt.

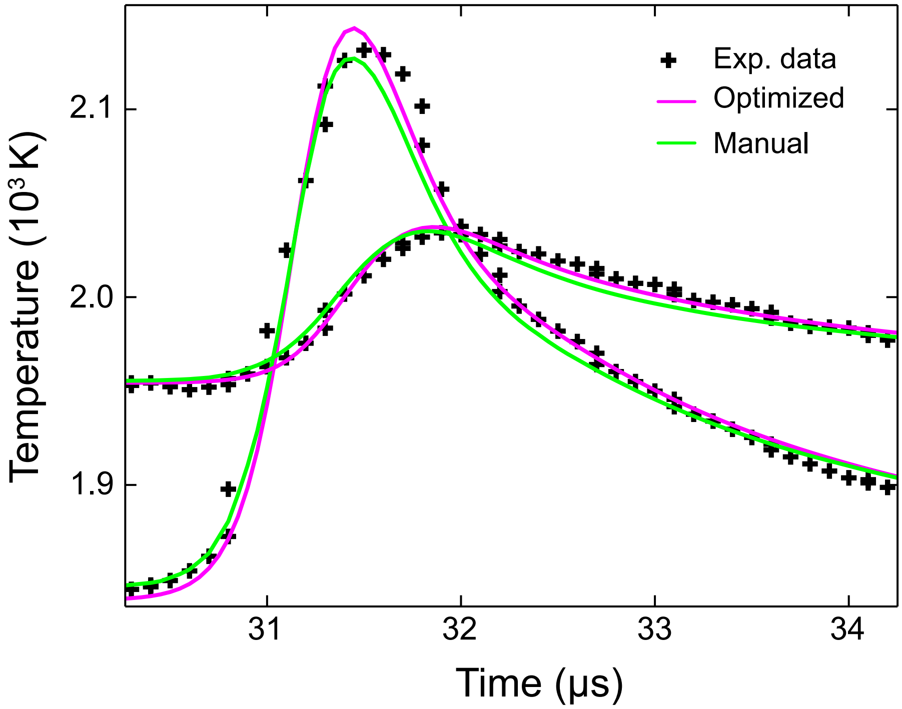

Extended Data Figure 5 | Comparison between manual and automatic optimization results for an experiment at 130 GPa. The manual approach, used as our primary fitting method, was based on an adjustment of model parameters by hand within a precision of ~5 W m^{-1} K^{-1}, giving $k = 45$ W m^{-1} K^{-1} and $k_{\mathrm{Ar}} = 60$ W m^{-1} K^{-1} as the best fit. The automatic result is the best fit based on a Levenberg–Marquardt least-squares minimization of model parameters, yielding $k = 38.6$ W m^{-1} K^{-1} and $k_{\mathrm{Ar}} = 50.4$ W m^{-1} K^{-1}. The automatic optimization obtained a better least-squares fit (χ^2 improved by 23%); however, the difference in k is not statistically significant.

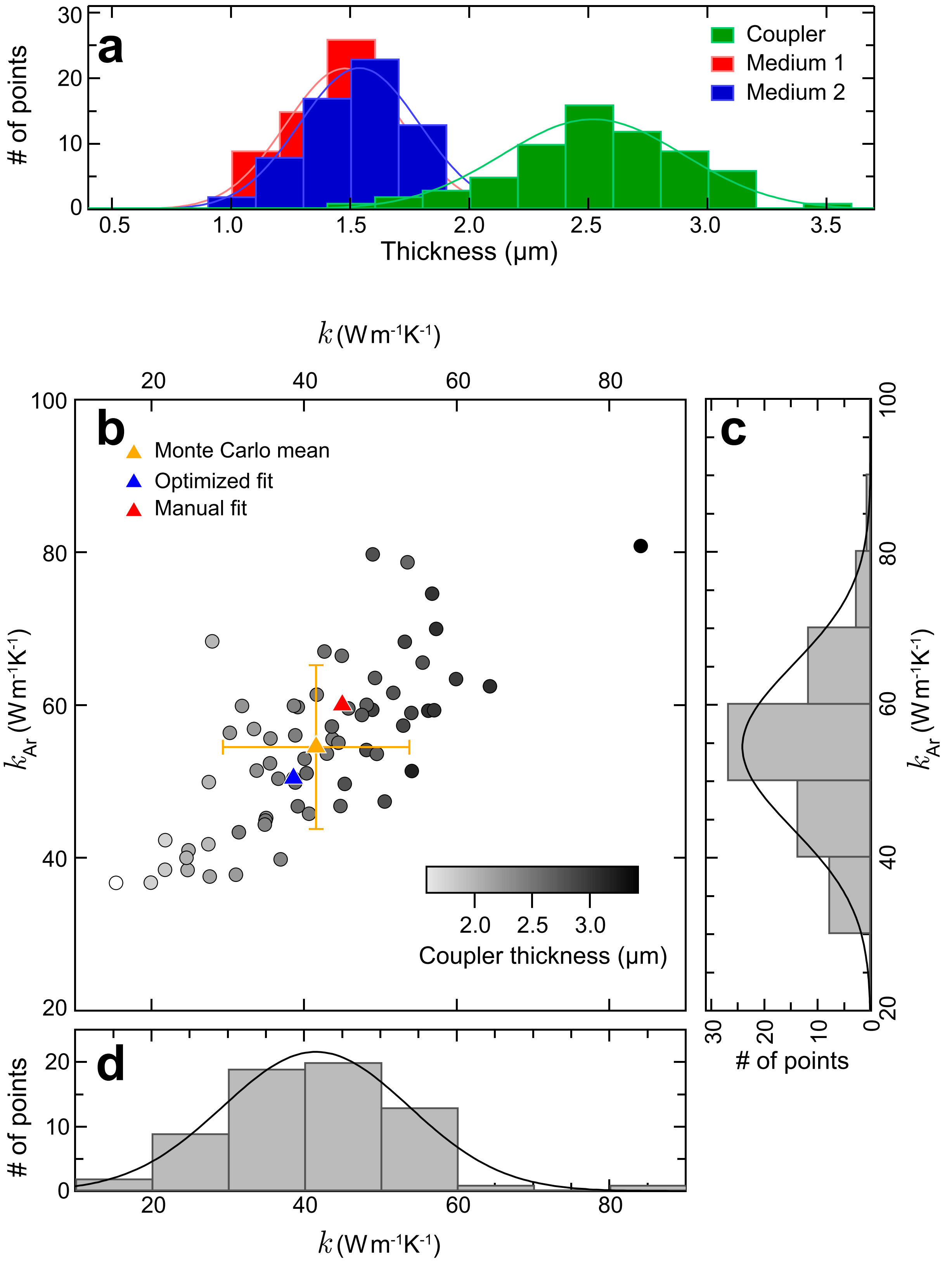

Extended Data Figure 6 | Monte Carlo analysis of error coupling in thickness uncertainties and effect on thermal conductivities, for the 130-GPa data set shown in Extended Data Fig. 5. a, Histogram showing randomly sampled thicknesses (upper and lower medium, and foil) in Gaussian probability distributions with standard deviation 30%. **b**, Thermal conductivities for Ar and Fe for 64 samples. The greyscale refers to the value of the coupler thickness, showing the correlation between high values for *k* and thicker coupler. The results of fits shown in Extended Data Fig. 5 are blue and red triangles, while the mean and one standard deviation found from the spread of sampled thermal conductivities is the orange triangle. **c** and **d** are histograms showing the distribution of thermal conductivities in **b**.

Extended Data Table 1 | Input parameters used for the finite-element modeling

P (GPa)	medium	sample thickness (μm)	pulsed side thickness (μm)	opposite side thickness (μm)	medium density (kg m^{-3})	C_p medium (J kg^{-1}K^{-1})	iron density (kg m^{-3})	C_p iron (J kg^{-1}K^{-1})
35	NaCl	3.0	8.0	7.0	3630	$\begin{cases} 748 + 0.34\,T, & T < 1000\text{K} \\ 1103, & T > 1000\text{K} \end{cases}$	9602	450
48	NaCl	2.9	7.4	6.7	3911	$\begin{cases} 748 + 0.34\,T, & T < 1000\text{K} \\ 1103, & T > 1000\text{K} \end{cases}$	9929	450
58	Ar	2.9	1.5	6.5	4539	570	10174	700
74	Ar	2.8	1.0	6.4	4800	570	10476	700
88	Ar	2.7	1.7	1.7	5057	570	10800	700
112	Ar	2.6	1.6	1.6	5326	570	11225	700
130	Ar	2.5	1.5	1.5	5550	570	11590	700

Extended Data Table 2 | Coefficients for the Grüneisen parameter and the isothermal bulk modulus used to estimate pressure variation of thermal conductivity

Coefficient for Grüneisen parameter		Coefficient for K_T	
a	1.76×10^{0}	K_1	97.50
b	2.04×10^{-2}	K_2	25.77
c	2.90×10^{-2}	K_3	-0.26
d	-1.32×10^{-4}		
e	-1.87×10^{-4}		
f	3.90×10^{-5}		
g	3.42×10^{-5}		
h	2.55×10^{-9}		
i	3.05×10^{-9}		
j	-5.10×10^{-7}		
k	-4.37×10^{-7}		